

Modelling and Development of Comb drive based RF MEMS switch for Nanosatellite Application

Neelima R. Kolhare, Associate Professor, Dept of E&TC, Government College of Engineering, Aurangabad, Maharashtra, India, Email: nilimageca@gmail.com

Dr. Ulhas Shinde, Principal, CSMSS Chh Shahu College of Engineering, Maharashtra, India.

Abstract - A non contact switch using comb drive actuator gives a fast on and off mechanism is controlled by electrostatic force. The switch is made up of silicon structure which is free from stiction problem. A electrostatic microactuator provides simplicity, low power, fast response, low cost. A $50\mu\text{m}$ width provides a high stiffness of the beam in the out of plane axis, therefore provides the switch with high reliability and stability. The experimental result shows that the isolation is 17.02db, insertion loss is -2.147db, Return loss is -12.146db at 10GHz and witching time is 197.73 μs .

Keywords —Comb drive, RF MEMS, Electomechanical modeling, Silicon wafer, CPW, COMSOL

I. INTRODUCTION

1.1 Design of contactless MEMS Switch

The proposed switch is a capacitive shunt type operated by the change of capacitance between the signal line and ground lines. As shown in Fig.1.1, the switch consists of a coplanar waveguide (CPW) line and variable capacitors. A couple of comb-drive actuators are linked with variable capacitors for precision actuation of the capacitor structures. The switching mechanism of the proposed switch is shown in Fig. 1.1. In the ON state, the variable capacitors are not actuated and the input signal passes through the CPW line, as shown in Fig. 1.1(a). In the OFF state, the capacitance of the actuated capacitors is changed and it prevents the signal from reaching the output port, as shown in Fig. 3.1(b). It is to be noted that there are small air gaps between the capacitors even in the OFF state. Therefore, the capacitors do not touch each other. Thus, the proposed switch is free from the stiction and microwelding problems of a contact-type switch. In order to have a sufficient capacitance of several hundred femtofarads in the OFF state, the comb structures are used in the variable capacitors and CPW line.

A. Transmission Line Design

The transmission line is formed from three parallel-plate wave guides running parallel to one another. This can be realized by forming $4\text{-}\mu\text{m}$ -thick evaporated copper on a released high-resistivity silicon (HRS) bridge with a large air gap. The schematic diagram of the transmission line is shown in Fig. 1.1 A $50\text{-}\Omega$ transmission line impedance can be obtained by adjusting the width of the CPW signal line S , the gap width between the signal line and ground line G , and the width of the ground line W . A commercial

simulation software application (COMSOL) has been used for this system. In addition, the dimensions of S , G , and W in this simulation are 100, 17, and $350\mu\text{m}$, respectively.

B. Variable Capacitor Design

The combs and bar structures of the variable capacitors are modeled with inductors and capacitors, as shown in Fig. 1.1(a). There are three types of inductors, namely, $L1$, $L2$, and $L3$

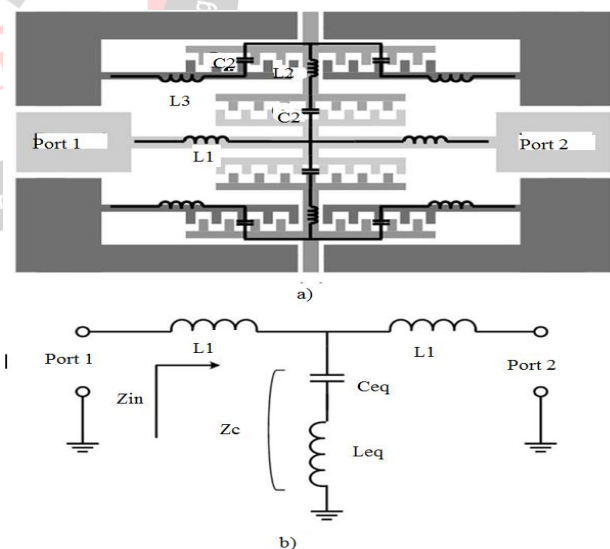


Figure 1.1 a) Proposed design of RF MEMS switch b) Electrical equivalent circuit

capacitors, namely, $C1$ and $C2$. Since the structure of the switch has vertical and horizontal symmetry, there are counterparts for the labelled inductors and capacitors. The simple equivalent circuit model of the switch is shown in Fig. 1.1(b). The equivalent circuit model contains all of the

overlapping counterparts. The equivalent inductance L_{eq} and the equivalent capacitance C_{eq} can be written as

$$L_{eq} = \frac{1}{2}L_2 + \frac{1}{4}L_3 \quad [3.1]$$

$$C_{eq} = \frac{4C_1.C_2}{C_1+C_2} \quad [3.2]$$

There should be a short circuit between the signal line and ground lines to obtain a high isolation in the OFF state. In addition, to obtain a low insertion loss in the ON state, the impedance, shown at port 1, should be 50Ω when port 2 is terminated in a matched load ($Z_0 = 50 \Omega$). There are several combinations of inductances and capacitances that satisfy (1) and (2) at 1000MHz.

The physical dimensions of the inductors and capacitors are determined by a full-wave simulation using the COMSOL program.

The actuation distance = $25 \mu\text{m}$.

The inductor L_1 =width of $40 \mu\text{m}$, a $t = 4 \mu\text{m}$, length = $360 \mu\text{m}$.

The inductor L_2 has the same cross-sectional area but lengths = $375 \mu\text{m}$ (OFF state) and $400 \mu\text{m}$ (ON state). It is more difficult to find the dimensions of the inductor L_3 than the other inductors because it is in the same space as C_2 . Therefore, the dimensions of C_2 are adjusted and the inductance of L_3 , approximately 0.19 nH , is calculated from the resonant frequency of C_2 and L_3 . $C_2 > C_1$, The width and the pitch of the comb fingers of C_1 are 2 and $7 \mu\text{m}$, respectively, and the width and the pitch of the comb fingers of C_2 are 2 and $10 \mu\text{m}$, respectively.

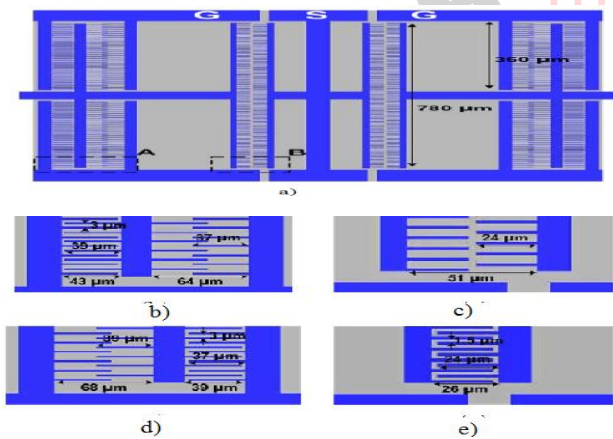


Figure 1.2 Three-dimensional example model and the determined dimensions of variable capacitor Structures

C. Actuator Design

In this report, i have used comb-drive actuator with folded springs for precision control of the switch displacement.

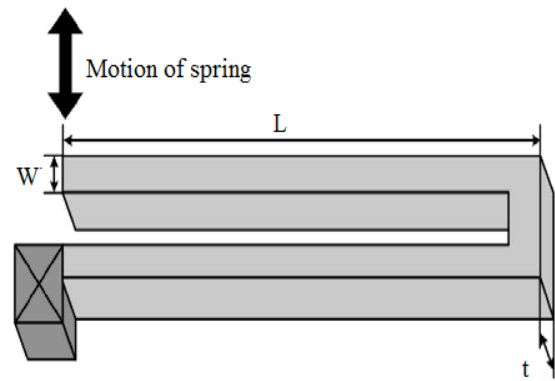


Figure 1.3 Schematic diagram of the mechanical spring.

Table 1.2 Detailed dimension of the comb drive actuator

		Designed dimensions
Comb finger	Number	5
	Thickness	$40 \mu\text{m}$
	Length	$27 \mu\text{m}$
Folded beam spring	Gap	$2.1 \mu\text{m}$
	Width	$5 \mu\text{m}$
	Thickness	$40 \mu\text{m}$
	Length	$200 \mu\text{m}$

variable capacitor is extended from the mass of the actuator. The relationship between the driving voltage and the displacement in the comb-drive actuator can be expressed as

$$F_k = \frac{2Et w^3}{L^3} d \quad [1.3]$$

where F_k is a restoring force, k is the mechanical spring constant, $E = 168.9 \text{ GP}$ is the Young's modulus, t is the spring and structure thickness, w is the spring width, L is the spring length, d is the stroke of the actuator, F_e is an electrostatic force, $\epsilon = 8.854 \times 10^{-12} \text{ F/m}$ is the permittivity, N is the number of combs, V is the switch control voltage, and g is the gap between moving combs and stationary combs. The schematic diagram of the mechanical spring is shown in Fig.1.3. The target actuation stroke is $25 \mu\text{m}$ as described in the variable capacitor design section. The spring length, the spring width, the structure thickness, and the gap between the combs are 650 , 5 , 40 , and $2.1 \mu\text{m}$, respectively, due to the fabrication issues. The control In order to analyze the actuation motion of the designed switch structure, finite element method (FEM) modelling on the switch structure is performed using COMSOL v4.1 voltage is set below 30 V , because the RF measurement system cannot withstand high voltage. The detailed dimensions of the comb-drive actuator, considering design factor and constraint, are summarized in Table3.2.

Within the former category, one finds that there exist mature, independently developed modeling tools addressing, on the one hand, the electromechanical behaviour of devices (e.g. ANSYS, ABAQUS, Intellisense, CoventorWare), and on the other hand, their electromagnetic behaviour (e.g., Ansoft Maxwell, Agilent HFSS). Under these circumstances (i.e., without an all encompassing single modeling tool), RF MEMS modelling may be predicated as shown in Figure 1.1

1.2 Specification of system

Table 1.1 Specification of system.

Actuation stroke	25µm
Actuation voltage	20 V
Switching time	197µsec
Operating frequency	1GHz-10GHz
Isolation (dB)	-17.02

1.3 MEMS Mechanical Modeling

The mechanical modeling process begins with a statement of the desired mechanical and electrical/microwave specifications of the device. Typical mechanical specifications include actuation voltage, mechanical resonance frequency, and contact forces; while typical electrical specifications include scattering parameters (insertion loss, return loss, and isolation), switching time, and power dissipation induced temperature rise.

Before detailed numerical simulation begins, approximate reduced order analytical models are used to arrive at an approximate baseline device structure from which numerical simulations can depart. The numerical simulation process begins with a layout of the device structure (i.e., its geometry, dimensions, and constituent materials). This description is combined with information on the fabrication process in order to emulate the effect of the process steps on the structure and to produce the 3-D solid model reflecting the process peculiarities. The solid model, thus obtained, is then meshed in preparation for the electro-mechanical finite element simulation. At this point the numerical model becomes a laboratory in itself, as number runs are undertaken to explore the dependence of intended performance measures, in the context of the design space, and to arrive at the specific device design that meets the mechanical specifications.

The design space typically includes geometry (i.e., structure length, width, and thickness), the dimensions of certain air gaps, the actuation area, and the effect of process-induced phenomena such as residual stress and stress gradients on performance.

In general, to design a RF MEMS electrostatic activated switch, the structure of the switch beam must be chosen so as to produce the lowest possible insertion loss, the highest possible isolation, the highest possible switching frequency, and lowest possible actuation voltage. The insertion loss will be affected by mismatch loss, which comes from the beam characteristic impedance being different from 50 Ω as well as losses in the beam metal and contact resistance loss. The beam-to-substrate separation that defines the parasitic capacitance, on the other hand, will affect the isolation. Table 1.2 lists the design goal of the MEMS switch in this work.

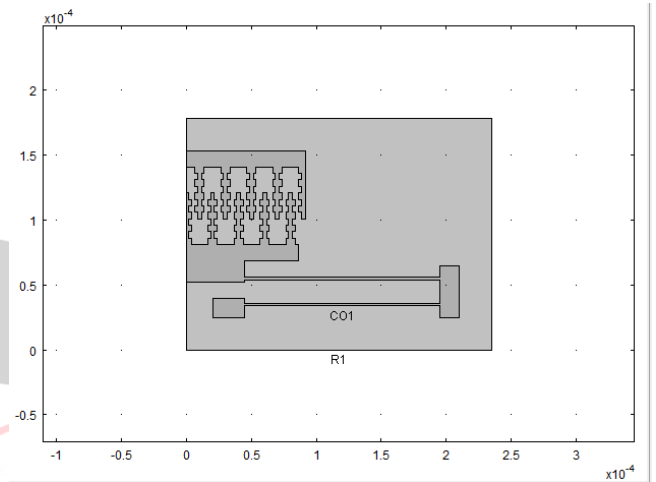


Figure 1.4 Mechanical modelling of proposed switch.

Figure 1.4 illustrates the basic design of a capacitive shunt switch using comb drive actuator by CAD software called COMSOL

The MEMS design involves: (1) design of a coplanar waveguide transmission line with $Z_0 = 50 \Omega$ characteristic impedance and short circuit gaps.

(2) design of a comb drive actuator with optimized spring constant, materials and beam gap height to reduce the activation voltage with reasonable isolation.

1.4 Working principle

The proposed switch is a laterally driven capacitive shunt switch operated by the change of the capacitance between the signal line and ground lines. The switch consists of a coplanar waveguide (CPW) line and variable capacitors and actuators. Electrostatic comb drive actuators are used for moving the variable capacitor parts in the lateral direction. The stoppers are used to limit the movement of the actuators, to prevent the contact of variable

capacitor metals Figure 1.5 contains the schematic diagram of the MEMS switch except the actuator regions and presents the on/off mechanism of the MEMS switch. The dark grey regions indicate fixed structures, and the bright grey regions indicate movable structures. Without applying a direct current (DC) bias across the actuators, the bright

grey regions do not move resulting in the on state of the switch. With a DC bias voltage over 25 V, the bright grey regions move close to the signal line resulting in the off state of the switch. The air gaps between the movable parts and the stationary parts of capacitors are 27 μm in the on state, and 2 μm in the off state. Thus, the actuator stroke is 25 μm with a 25 V DC applied voltage.

The proposed switch is designed to be safe from contact failures, RF latching, and RF self-actuation

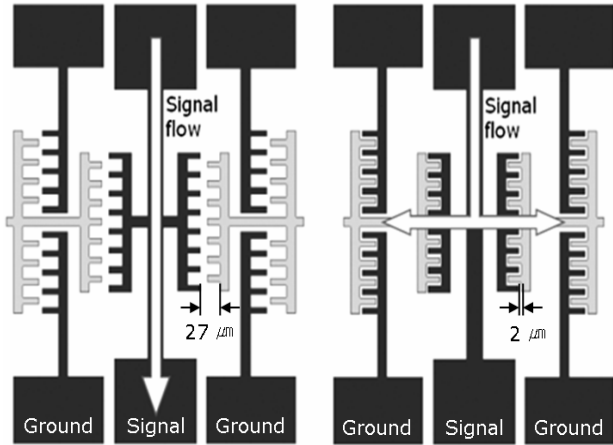


Figure 1.5 On/off mechanism of switch.

The combs and bar structures of the variable capacitors are modeled with inductors and capacitors. According to the physical dimension of the combs and bar structures the values of the inductors and the capacitors are adjusted.

1.5. Design consideration

1.5.1. Design of a Coplanar Waveguide

Coplanar waveguide (CPW) is-conductor transmission line. Coplanar waveguide G-S_ An e formula for the characteristic impedance, $0 < k < 1$, and $h \gg w$, is

$$Z_0 = \frac{30\pi^2}{\sqrt{(\epsilon_r+1)/2}} \left[\ln\left(2 \frac{1+\sqrt{k}}{1-\sqrt{k}}\right) \right] \quad [3.4]$$

Where, $k = \frac{w}{w+2s}$

w=center strip width,s=slot width

ϵ =relative dielectric constant of the dielectric substrate

An empirical equation for effective relative dielectric constant ϵ_{re} of Eq. 1.4 is

$$\epsilon_{re} = \frac{\epsilon_r+1}{2} \left[\tanh\left(1.785 \log \frac{h}{w} + 1.75\right) + \frac{kw}{h} (0.04 - 0.7k + (1 - 0.1\epsilon_r) \frac{(0.25+k)}{100}) \right] \quad [1.5]$$

As shown in Figure 3.3, the Silicon substrate of $\epsilon_r = 11.8$ was chosen, and CPW center conductor width $w = 20 \mu\text{m}$ and ground spacing $s = 11.8 \mu\text{m}$, nearly thickness is 1 mm

and nearly infinite compared to width. The effective dielectric constant is 6.4.

Figure 3.7 illustrates the optimized 3D view of CPW and CPW with 20 μm (b) and 40 μm separation for the insertion loss, isolation, and switching frequency and return loss. The insertion loss is due to mismatch the characteristic impedance of the line and switch. The schematic diagram of the transmission line is shown in Fig.3.1. 50-Ω transmission line impedance can be obtained by adjusting the width of the CPW signal line S , the gap width between the signal line and ground line G , and the width of the ground line W . A commercial simulation software application (COMSOL) has been used for system. In addition, the dimensions of S , G , and W in this simulation are 166, 17, and 350 μm, respectively

1.5.2. Activation Mechanism

Electrostatic Actuation

When the voltage is applied between a fixed-fixed or cantilever beam and the pull down electrode, an electrostatic force is induced on the beam. The electrostatic force applied to the beam is found by considering the power delivered to a time-dependent capacitance and is given by

$$F_e = \frac{1}{2} V^2 \frac{dC(g)}{dg} = - \frac{1}{2} \frac{\epsilon_0 W w V^2}{g^2} \quad [1.6]$$

where V is the voltage applied between the beam and electrode.

Ww is the electrode area.

The electrostatic force is approximated as being distributed evenly across the beam section above the electrode. Equating the applied electrostatic force with the mechanical restoring force due to the stiffness of the beam ($F = Kx$),

$$F_k = \frac{2Et w^3}{L^3} d \quad [1.7]$$

Where F_k =restoring force

$$F_k = \frac{2 \times 168.9 \times 40 \times 10^{-6} \times 5 \times 10^{-6}}{200 \times 10^{-6}} = 25 \times 10^{-6}$$

$$F_k = 2.59 \times 10^{-6} \text{ N}$$

$$\text{displacement} = \frac{F}{K}$$

Where K is a spring constant

$$= \frac{2.59 \times 10^{-6}}{4.7} = 5.51063 \times 10^{-7}$$

Similarly by putting the values in above equation we get ,

Actuation voltage(v)	Displacement (10^{-10})
----------------------	-----------------------------

	Theoretical	Simulation result
100	5.5106	5.5
200	5.9101	6.0
300	6.2109	6.5
400	6.9101	7.0

Table 3.3 Theoretical and practical analysis.

Where g_0 is the zero-bias bridge height. At $(2/3g_0)$, the increase in the electrostatic force is greater than the increase in the restoring force, resulting in the beam position becoming unstable and collapse of the beam to the down-state position. The pull-down (also called pull-in) voltage is found to be

$$V_p = V \left(\frac{2g_0}{3} \right) = \sqrt{\frac{8k}{27\epsilon_0 W_w}} g_0^3 = \sqrt{\frac{8k}{27\epsilon_0 A}} g_0^3 \quad [1.8]$$

$E=169 \text{ GPa}$

$h= 3\mu\text{m}$

$b=50 \mu\text{m}$

$d=1 \mu\text{m}$

beam length= $100 \mu\text{m}$

poisson's ratio= 0.32

then, $V_p = 39.9V$

Beam length= $150 \mu\text{m}$

Poisson's ratio= 0.06

then, $V_p = 16.8V$

As shown in Eq. (1.8), the pull down voltage depends on the spring constant of beam structure, and, beam gap g_0 and electrode area A . To reduce the actuation voltage, the key is beam structure of low spring constant k . The pull-in voltage was investigated in terms of beam structure (different k), beam thickness, gap and beam materials.

Design of low spring constant (k)

Fixed-fixed beam with different spring constants considered in this report are shown in Figure 3.4. As shown, Figure 1.9 (a) is a fixed-fixed beam; the spring constant is calculated to be 16.6 N/m for Gold; Figure 1.9(b), (c) and (d) are low k design with meander structures. The spring constant k calculation of such beam structures can be complicated and details of the most commonly used low k beam design for MEMS application and the relevant equations of spring constant k are included. The spring constant k of structure (b) and (d) is estimated to around 5.91 N/m and structure (c) is $2\sim 3 \text{ N/m}$.

Materials	Young's modulus,E	Poisson ratio,v	Electrical conductivity $S\text{m}^{-1}$
Gold (Au)	57	0.35	45.16×10^6
Copper (Cu)	128	0.36	59.16×10^6
Nickel(Ni)	180	0.31	14.4×10^6
Aluminium(Al)	77	0.3	37.8×10^6

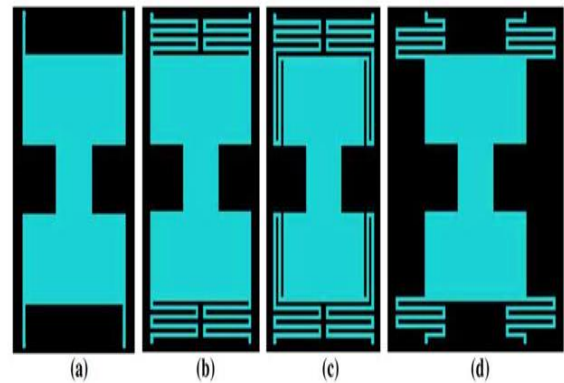


Figure 1.7 The beam structure of different spring constant.

In this project, I have used a simple cantilever beam. The structure of this beam is shown in fig.1.10, which consists of a fixed anchor at one end and the spring is connected to another end.

A load is applied at fixed anchor.

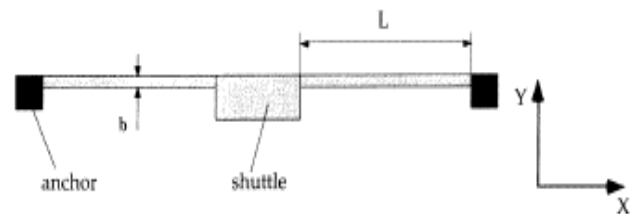


Figure 1.8 Beam structure of proposed non contact switch.

In this project I have selected such dimensions of cantilever beam so that which minimizes the spring constant. The dimensions of parameters are:

$E=168.9, l=200 \mu\text{m}, t=1 \mu\text{m}, w=50 \mu\text{m}, g=2.1 \mu\text{m}$

$$k = 32Ew \left(\frac{t}{l} \right)^3 \quad [1.9]$$

After putting the above values in eq. [3.9] we get, $k=3.378 \text{ N/m}$.

Table 1.4 Material properties

Beam Materials

The metal beam needs to sustain the major mechanical deflection and be a perfect conductor. Gold, Copper, Nickel and Aluminum are most commonly used electrical materials in microfabrication and chosen due to their Young’s Modulus, electrical conductivity and manufacturability. Table 3.4 shows the materials properties of these materials.

3.6 Model definition

Figure shows the microtweezers (top) and a close-up of part of the comb drive (bottom). Applying a voltage across the gaps between the combs actuates the tweezers. The structure is made of polysilicon and has a thickness of a few micrometers.

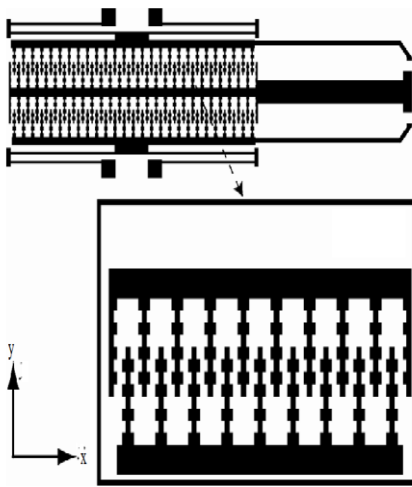


Figure 1.9 The microtweezers (top) and the comb-drive mechanism (bottom).

The model includes just a few of the teeth. It simulates only the comb drive and its attachment using double-folded beam springs. Taking advantage of symmetries means that you only have to set up a quarter of the geometry, see Figure 1.9

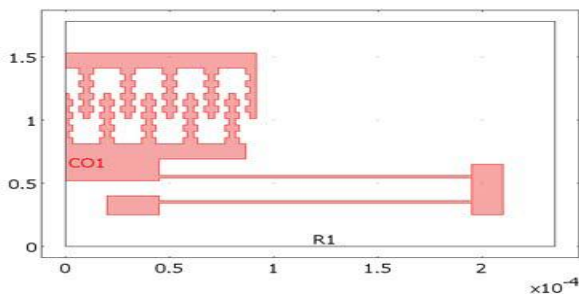


Figure 1.10 Initial (undeformed) model geometry.

The upper half of the comb is fixed, as is the end of the beam spring. The system applies an electric potential to the beam spring and the lower comb; the upper comb is grounded. In the air surrounding the comb drive, the model solves the electrostatic equation

$$-\nabla \cdot (\epsilon \nabla V) = 0.$$

The electrostatic force density is

$$F_{es} = \frac{\epsilon E^2}{2},$$

and the simulation applies it to each comb as a perpendicular boundary load.

Modeling in COMSOL Multiphysics

Because electrostatic forces attract the combs to each other, any geometric change has an impact on the electric field between them. To account for this effect, the model uses an arbitrary Lagrangian-Eulerian (ALE) method implemented in COMSOL Multiphysics’ Moving Mesh application mode. This application mode automatically keeps track of the movements and translate application mode equations between the fixed (reference) and moving frames.

In this model the displacements are relatively large. Therefore, i am using the Plane Stress application mode’s support for large deformations. To define the electrostatic force, i am using the Electrostatics application mode’s Maxwell surface stress tensor boundary variables. The geometry of this model is rather complex and thus the boundary conditions are laborious to enter. For an example that is faster and easier to set up.

Modeling Using the Graphical User Interface

MODEL NAVIGATOR

Structural Mechanics:Static analysis.

Name	Width	Height	X	Y
R1	7	5	-3.5	81
R2	3	5	-1.5	86
R3	7	5	6.5	106
R4	3	5	8.5	101

Data	expression
X displacement	20
Y displacement	10
X size	5
Y size	4

Name	Width	Height	X	Y
R1	91.5	60	0	81

Name	Width	Height	X	Y
R1	91.5	12	0	141
R2	86.5	12	0	69
R3	45	17	0	52
R4	150	2	45	54
R5	150	2	45	54
R6	25	15	20	25
R7	15	40	195	25

Name	Width	Height	X	Y
R1	235	178	0	0

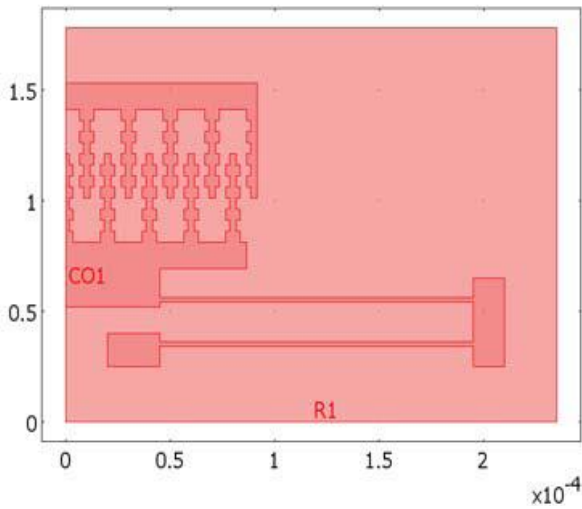


Figure 1.11 The completed comb-drive geometry.

Electrostatics analysis

Boundary Conditions—Electrostatics

Enter the settings in the following table. Note that the physical boundaries of the upper comb are all grounded, while those of the lower comb have an electric potential of V_{in} . The arms and the contact pads of the lower comb are electrically inactive. When you have entered all boundary conditions click the Groups tab and enter the group names. This helps us identify the boundaries if you want to make changes to the model.

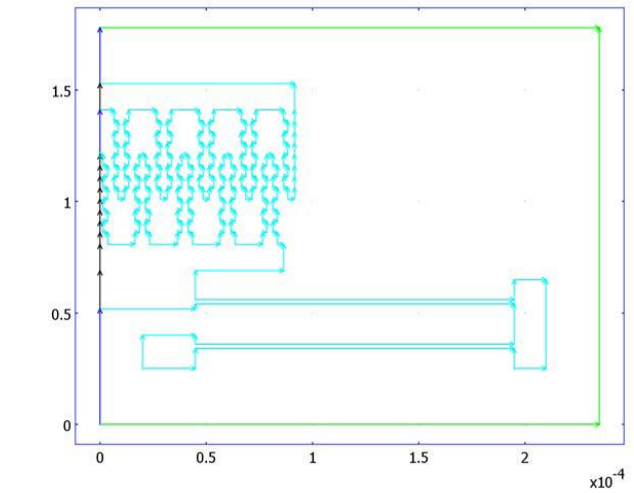


Figure 1.13 Moving mesh

Property	Value
E	168e9
ν	0.22
thickness	2e-6

The thermal expansion coefficient (α) is needed only if you have included thermal expansion in the load settings. Similarly, the density (ρ) is used only in time-dependent, eigen frequency, and frequency-response analyses. In this case you use a nonlinear parametric analysis, and it is therefore not necessary to enter these values.

Boundary Conditions—Plane Stress

- 1 Open the Boundary Settings dialog box and make sure that the Interior boundaries check box is not selected.
- 2 On the Constraint and Load pages, define boundary conditions according to the following table. On the Load page, click the Edge load is defined as load/area using the thickness option button. This makes the loads from the Electrostatics application mode match the structural loads.

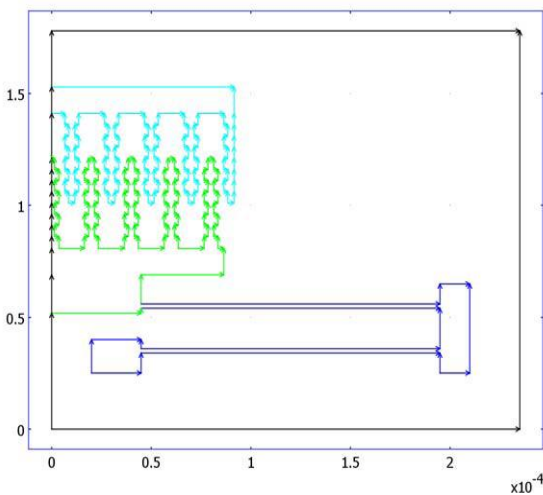


Figure 1.12 Boundary selection of actuator.

the Physics included displacement check box. For the displacement variables dx and dy , enter the values u and v , respectively. These variables represent the displacements calculated in the Plane Stress application mode.

Boundary Conditions—Moving Mesh

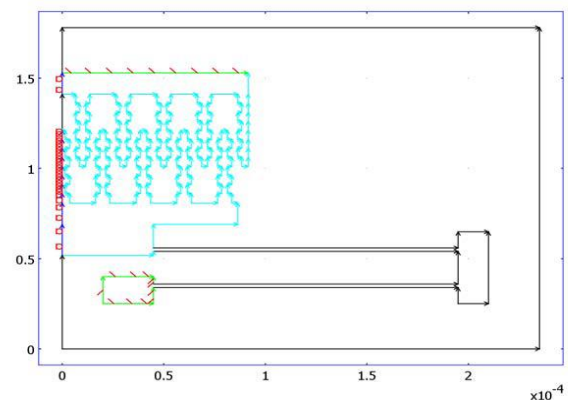


Figure 1.14 Applied geometry to system.

Mesh generation

Free Mesh Parameters.

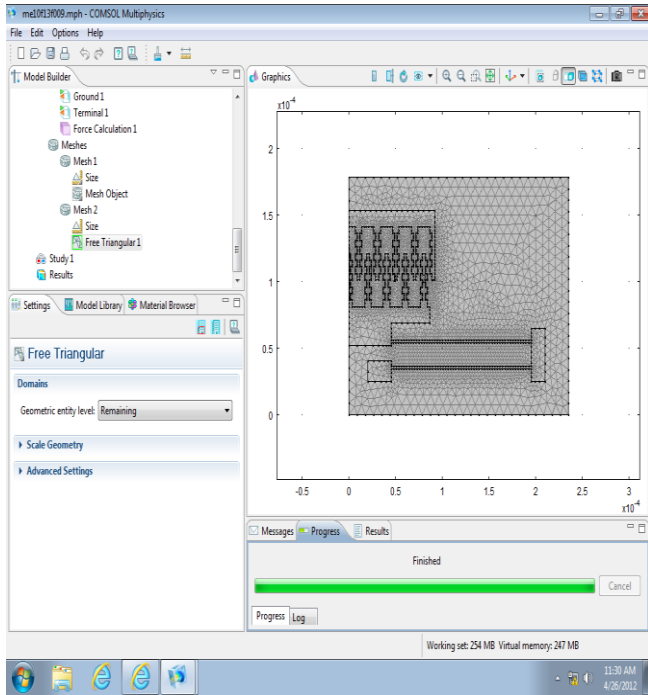
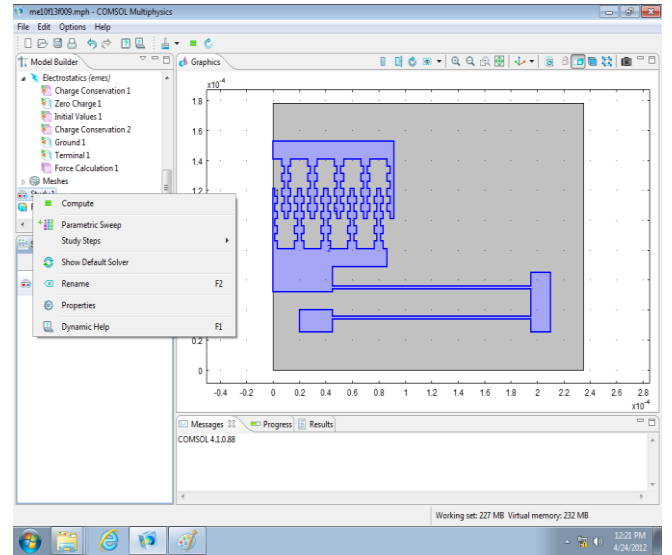


Figure 1.15 System after meshing process.

Postprocessing and Visualisation

The default results show von Mises stresses with colors on the deformed shape for the last parametric value, $V_{in}(12) = 600$ V. To study the electric potential in the moving frame do the following:

The resulting plot is reproduced in Figure 3.16.



22. To view result go to study and compute it we get a FEM analysis as shown below.

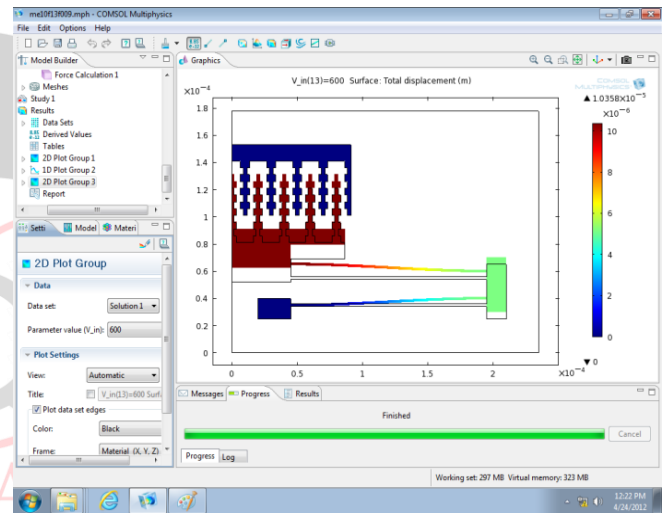


Figure 1.18 Major processing steps of the contactless MEMS switch. (a) Coplanar waveguide; (b) Dielectric layer on the actuation electrodes; (c) switching beam.

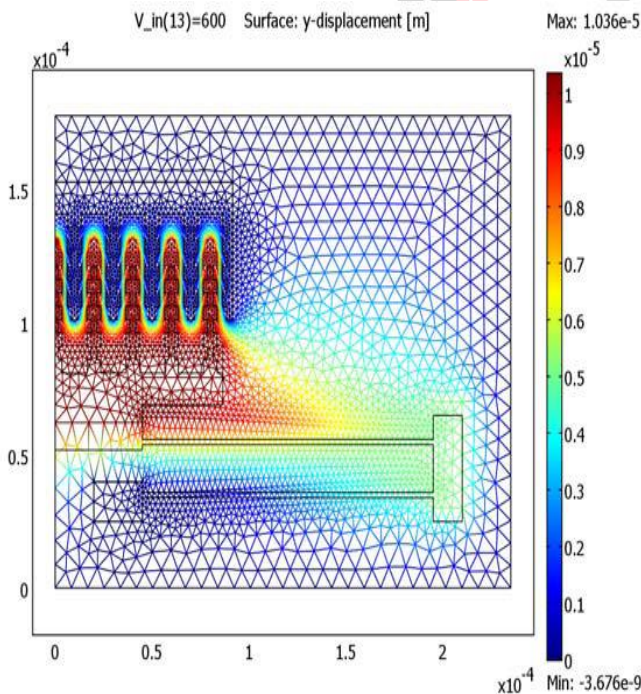


Figure 1.16 Meshed geometry.

II. ELECTROMECHANICAL MODELLING OF RF MEMS SWITCH

The electromechanical analysis starts with simulation on electrical field distribution and calculation of the electrostatic force F_{es} . and V_x , V_y , and V_z are the electrical field components in x, y and z direction. With this F_{es} acting on the beam and counter balancing of restoring force from spring constant k , the deflection of the beam can be calculated. F_{es} distribution along the y-axis in the simple beam and meander1 configuration respectively. As shown, the F_{es} is acting on the beam region facing the bottom electrodes and the beam is elastically deformed. The whole beam was pulled upwards and as expected, the larger the activation voltage, the more deflection the beam exhibits. F_{es} is much higher for meander structures due to increase in

electrode area, therefore, a more deflection can be generated for meander at lower activation voltage.

$$F_{es} = \frac{2 \times 168.9 \times 40 \times 10^{-6} \times 5 \times 10^{-6}}{200 \times 10^{-6}} 25 \times 10^{-6} \quad [2.1]$$

$$F_{es} = 2.59 \times 10^{-6} N$$

It is known that for the parallel-plate capacitance, $C = \epsilon \times A/d$ where A is the underlying area of the parallel plates and d is spacing.

$$C_{max} = \frac{3\epsilon_0 A}{2g} \quad [2.2]$$

Putting $\epsilon_0 = 8.854 \times 10^{-12} F/m$

$$C_{max} = 4.7432 \times 10^{-16} F$$

$$C_{min} = \frac{3\epsilon_0 A}{4g} \quad [2.3]$$

$$C_{min} = 3.5574 \times 10^{-16} F$$

When the switch is in the up state, and spacing between beam bridge and fingers remains same, only thing changes with meander structure is the underlying area between beam and electrode.

2.1.1 Switching time of switch: it is a time at which switch becomes comes into on state after few microseconds goes into off state this time is called as switching time.

Switching time of proposed switch is calculated as follows:

$$\omega_0 = \sqrt{\frac{k}{m}} \quad [2.4]$$

Where m is a effective mass of beam(2)

k is spring constant(3.378N/m) putting into eq.[2.4]

V_s is 1.4 times of V_p .

$$t_s = 3.67 \frac{V_p}{V_s \omega_0} \quad [2.5]$$

After putting all the values into eq.[2.5] we get switching time is equal to 197µsecond.

2.1.2 Modal Analysis of Switch Beam

Any physical system can vibrate. The frequencies at which vibration naturally occurs, and the modal shapes that the vibrating system assumes are properties of the system, and can be determined analytically using Modal Analysis. Modal analysis computes the resonant frequencies of the switch beam at equilibrium. At these resonance frequencies, the switch beam tends to response to a bounded excitation with an unbounded response, i.e., the system transfer function becomes infinite at the resonance frequency. These frequencies and their associated mode shapes are of

particular interest in design because they are closely resemble the corresponding characteristics of an underdamped mechanical system, and they indicate when the system will have its maximum response to an intended or unintended (noise) input. In the case of switch beam, the switch speed should be well below the first resonance frequency to avoid displacement peak. The design goal is to increase the beam structure mode 1 resonance frequency.

Modal analysis of the switch beam was performed using COMSOL and mode shapes are shown in Figure 2.1

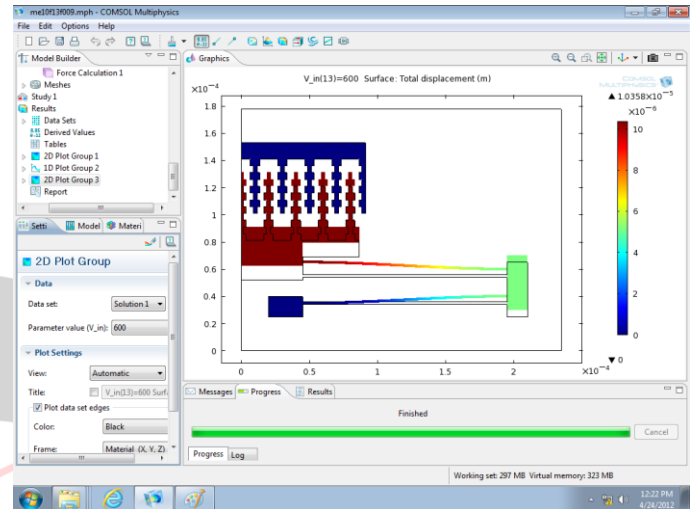


Figure 2.1 modal analysis of system.

Sr. no.	Actuation voltage	displacement
1	100	5.5×10^{-10}
2	200	6×10^{-10}
3	300	6.5×10^{-10}
4	400	7×10^{-10}
5	500	7.5×10^{-10}
6	600	8×10^{-10}

Table 2.1 Simulation result.

The upper half of the comb is fixed, as is the end of the beam spring. The system applies an electric potential to the beam spring and the lower comb; the upper comb is grounded. In the air surrounding the comb drive, the model solves the electrostatic equation. Because electrostatic forces attract the combs to each other, any geometric change has an impact on the electric field between them. To account for this effect, the model uses an arbitrary Lagrangian-Eulerian (ALE) method implemented in COMSOL Multiphysics' Moving Mesh application mode. This application mode automatically keeps track of the movements and translate application mode equations between the fixed (reference) and moving frames.

In this model the displacements are relatively large shown in fig 2.3. Therefore, i am using the Plane Stress application mode's support for large deformations. To define the electrostatic force, i am using the Electrostatics application mode's Maxwell surface stress tensor boundary variables.

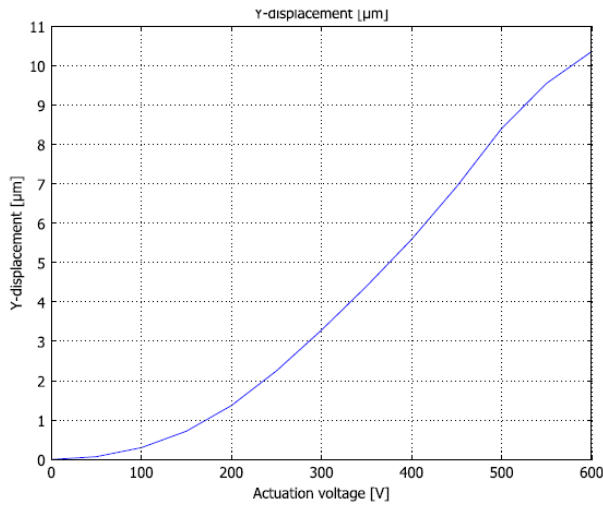


Figure 2.2 A graph of actuation voltage vs displacement.

2.2. Electromagnetic modelling of RF MEMS switch

Electromagnetic modelling of coplanar waveguide transmission line and RF MEMS shunt switch will be investigated in the terms of the scattering parameters, i.e. S-parameter, electromagnetic software package. Simulation is to be first done on the continuous CPW and shorted CPW with two different separation gap 20 µm and 40 µm, followed by CPW with MEMS switch ON state.

1.2.1 Fitting CLR Parameter to S-parameter shunt capacitive switch measurements

$$S_{11} = \frac{-j\omega C_u Z_0}{2+j\omega C_u Z_0} \quad [2.4]$$

$$S_{21} = \frac{1}{1+j\omega C_d Z_0/2} \quad [2.5]$$

Table 2.2 S-parameter calculation.

Frequency (MHz)	RLin (dB)	S ₂₁ (dB)
1000	0.964	-13.514
2000	1.734	-10.061
3000	2.384	-8.898
4000	2.841	-8.473
5000	3.098	-8.543
6000	3.110	-9.193
7000	2.999	-10.257
8000	3.036	-11.634
9000	2.757	-13.893
10000	2.147	-17.016

After changing a material that is silicon ,we get isolation poorer as shown in comparison table .3 shown below.

If we compare both of the table then we can say that at lower frequency aluminium material is gives a better isolation but as demands increases that means as the frequency increases silicon material gives a better response.

Frequency(MHz)	S ₂₁ (dB)
1000	27.96
2000	23.48
3000	21.21
4000	19.83
5000	18.94
6000	18.49
7000	18.13
8000	18.06
9000	17.52
10000	16.71

Table 4.3 S-parameter using Al material.14.2.2

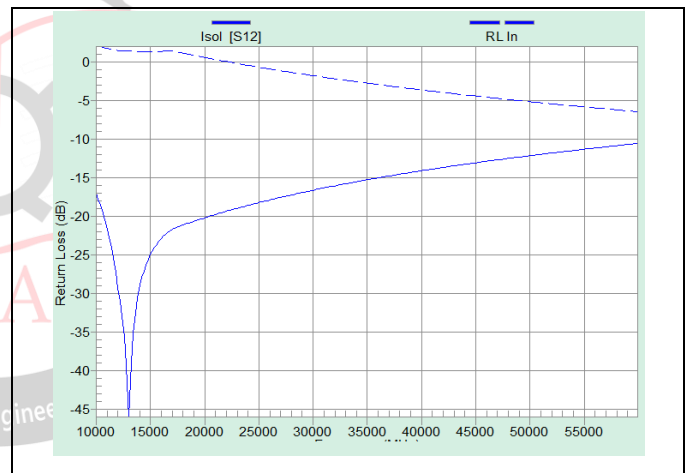


Figure 2.3 S-parameters of the EM simulated model

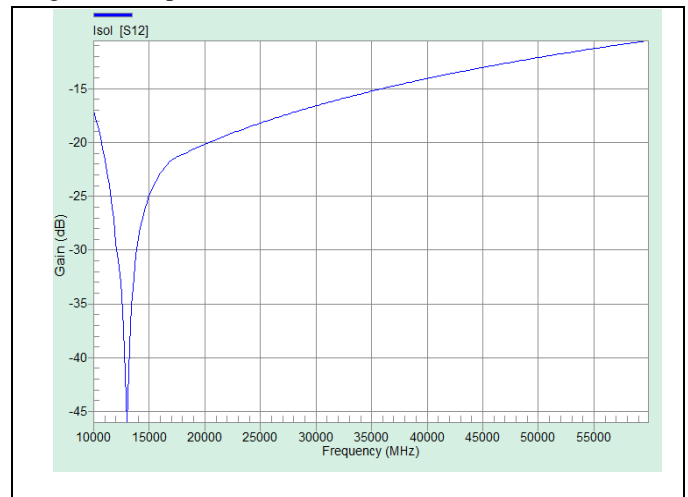


Figure 2.4 RF MEMS switch isolation graph.

III. CONCLUSION

1. There are a variety of excellent RF MEMS switches available in industry and university labs. Electrostatic actuation dominates the design of switches, but thermal or magnetostatic actuation is also available. Thermal switches can result in very large contact forces at the expense of 40–200 mW of DC power. The switching time is between 1 and 8000 ms, depending on the design.

2. Every switch is fabricated using a dedicated thin-film process, and most of these processes are not compatible with each other. However, most RF MEMS switches are compatible with post-CMOS and post-GaAs fabrication techniques.

3. MEMS metal-to-metal (DC) contact and capacitive switches have both been cycled to >50 billion cycles, and there is no reason why they should not be able to achieve >100 billion cycles at low-power levels (0.1–10 mW).

A non contact switch using comb drive actuator gives a fast on and off mechanism is controlled by electrostatic force. The switch is made up of silicon structure which is free from stiction problem. A electrostatic microactuator provides simplicity, low power, fast response, low cost. A 50 μ m width provides a high stiffness of the beam in the out of plane axis, therefore provides the switch with high reliability and stability. The experimental result shows that the isolation is 17.02db, insertion loss is -2.147db, Return loss is -12.146db at 10GHz and witching time is 197.73 μ s.

REFERENCES

- [1] Rohde UL, Newkirk DP (2000) RF/Microwave circuit design for wireless applications. Wiley, New York
- [2] J. U. Duncombe, "Infrared navigation—Part I: An assessment of feasibility (Periodical style)," *IJREAM Trans. Electron Devices*, vol. ED-11, pp. 34–39, Jan. 1959. Zavracky PM, McGruer NE, Morrison RH, Potter D (1999) Micro switches and micro relays with a view toward microwave applications. *Int J RF Microw Comput Aided Eng* 9:338–347
- [3] Hyman D, Lam J, Warneke B, Schmitz A, Hsu TY, Brown J, Schaffner J, Walston A, Loo RY, Mehregany M, Lee J (1999) Surfacemicromachined RF MEMS switches on GaAs substrates. *Int J RF Microw Comput Aided Eng*
- [4] Gong S, Shen H, Bark NS (2009) A cryogenic broadband DC contact RF MEMS switch. In: IEEE MTT-S International Microwave Symposium Digest, Boston, 7–12 June 2009, pp 1225–1228
- [5] Hou Z, Liu Z, Hu G, Liu L, Li Z (2006) Study on the reliability of capacitive shunt RF MEMS switch. In: 2006 7th international conference on electronics packaging technology
- [6] S Hwang JCM (2007) Reliability of electrostatically actuated RF MEMS switches. In: RFIT 2007-IEEE international workshop on radio-frequency integration technology, Singapore, 9–11 Dec 2007
- [7] Yao JJ (2000) RF MEMS from a device perspective. *J Micromech Microeng* 10(4):R9–R38
- [8] PandhariPande VM et al (2011) A non-contact type RF MEMS switch to remove stiction problem. *IEEE*
- [9] G. Legtenberg R, Groeneveld AW, Elwenspoek M (1996) Combdrive actuators for large displacements. *J Micromech Microeng* 6:320
- [10] Tang WC (1990) Electrostatic comb drive for resonant sensor and actuator applications. Doctoral dissertation